Multiphysics response of polycrystalline materials: Computational homogenization via the Virtual Element Method

C. Böhm, B. Hudobivnik,
M. Marino, P. Wriggers

Institute of Continuum Mechanics,
Leibniz Universität Hannover

May 17th to 19th, 2021

INdAM Workshop
Polygonal methods for PDEs:
theory and applications

Contents

Motivation - Why VEM for crystalline Environments

- Crystalline environments are geometrically heterogeneous
- Require partially higher mesh refinements to maintain accuracy

⇒ Virtual Elements provide abilities to fit grain-geometries perfectly [2]

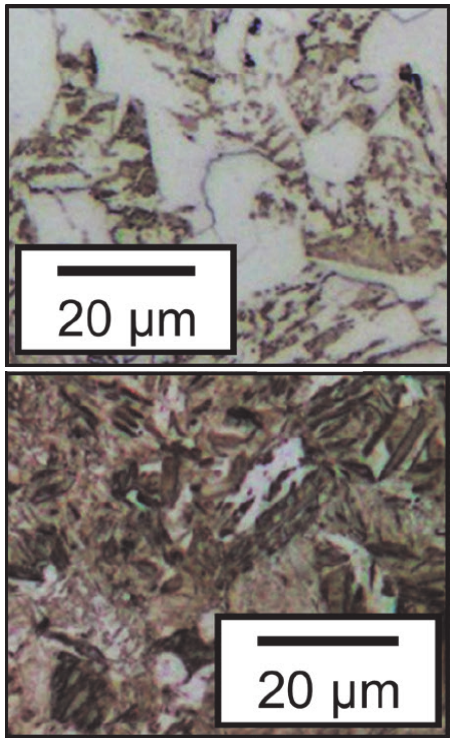

Fig. 1 Micrographs of induction-hardened steel-aluminum rods [1]

Constitutive Framework: Primary fields & governing equations

Introduction of primary variables:

$\mathcal{R} = \{\mathbf{u}, \phi, \varphi\}$

$$\underbrace{\boldsymbol{\varepsilon} = \frac{1}{2}\left(\nabla\mathbf{u} + (\nabla\mathbf{u})^{\mathrm{T}}\right)}_{\text{strain}}, \underbrace{\mathbf{E} = -\nabla\phi}_{\text{electric field}}, \underbrace{\mathbf{H} = -\nabla\varphi}_{\text{magnetic field}}$$

Grain-specific elastic energy function: $\Rightarrow \psi_g\left(\boldsymbol{\varepsilon}, \mathbf{E}, \mathbf{H}; \mathbf{R}_g\right)$

Governing equations:

$\mathrm{div}\left(\boldsymbol{\sigma}\right) = \mathbf{0}$	balance of linear momentum
$\mathrm{div}\left(\mathbf{D}\right) = Q$	Gauss's law of electro-statics
$\mathrm{div}\left(\mathbf{B}\right) = 0$	Gauss's law of magneto-statics

Constitutive Framework: Grain-specific elastic potential

Assumption: Arbitrary rotated grains

$\psi_g = \frac{1}{2}\mathbf{P} \cdot \mathbb{G}_g \cdot \mathbf{P}, \ \mathbf{P} = \mathrm{vec}\{\boldsymbol{\varepsilon}, \mathbf{E}, \mathbf{H}\}$

$\Rightarrow \mathbb{G}_g = \mathbf{R_L} \mathbb{G} \mathbf{R_P}$

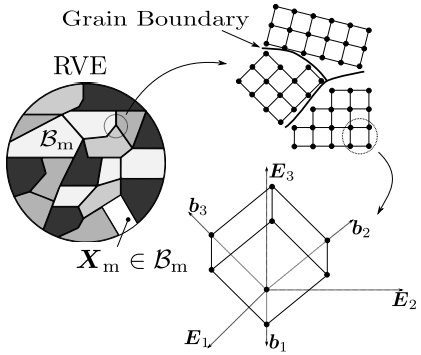

Fig. 3 Illustration of a face centered cubic unit cell, rotated against the global system $\{\mathbf{E}_1, \mathbf{E}_2, \mathbf{E}_3\}$

Micro-mechanical modulus $\mathbb{G}$[3]:

$$\boxed{\mathbb{G} = \begin{bmatrix} \mathbb{C} & -\mathbf{e}^\mathrm{T} & -\mathbf{q}^\mathrm{T} \\ -\mathbf{e} & -\boldsymbol{\epsilon} & -\boldsymbol{\alpha}^\mathrm{T} \\ -\mathbf{q} & -\boldsymbol{\alpha} & -\boldsymbol{\mu} \end{bmatrix}}$$

Element residual & element tangent matrix are computed via automated differentiation tool AceGen[4]: $\mathbf{R}_e = \frac{\partial \psi_g}{\partial \mathrm{vec}\{\mathcal{R}\}}, \ \mathbf{K}_e = \frac{\mathrm{D}\mathbf{R}_e}{\mathrm{D}\mathrm{vec}\{\mathcal{R}\}}$

Constitutive Framework: Computational homogenization

Based on the fulfilment of Hill's condition[3]:

$$\langle \boldsymbol{\sigma} : \varepsilon \rangle - \langle \mathbf{D} \cdot \mathbf{E} \rangle - \langle \mathbf{B} \cdot \mathbf{H} \rangle = \bar{\boldsymbol{\sigma}} : \bar{\varepsilon} - \bar{\mathbf{D}} \cdot \bar{\mathbf{E}} - \bar{\mathbf{B}} \cdot \bar{\mathbf{H}}, \ \langle \cdot \rangle = \bar{(\cdot)} = \frac{1}{V} \int_\Omega (\cdot) \mathrm{d}V$$

Yields macroscopic homogenized material matrix $\bar{\mathbb{G}}$:

$$\boxed{\bar{\mathbb{G}} = \begin{bmatrix} \bar{\mathbb{C}} & -\bar{\mathbf{e}}^{\mathrm{T}} & -\bar{\mathbf{q}}^{\mathrm{T}} \\ -\bar{\mathbf{e}} & -\bar{\boldsymbol{\epsilon}} & -\bar{\boldsymbol{\alpha}}^{\mathrm{T}} \\ -\bar{\mathbf{q}} & -\bar{\boldsymbol{\alpha}} & -\bar{\boldsymbol{\mu}} \end{bmatrix}}$$

with

$$\bar{\mathbb{C}} = \frac{\partial \langle \boldsymbol{\sigma} \rangle}{\partial \bar{\varepsilon}}, \ \bar{\mathbf{e}} = \frac{\partial \langle \mathbf{D} \rangle}{\partial \bar{\varepsilon}}, \ \bar{\mathbf{q}} = \frac{\partial \langle \mathbf{B} \rangle}{\partial \bar{\varepsilon}}, \ \bar{\boldsymbol{\epsilon}} = \frac{\partial \langle \mathbf{D} \rangle}{\partial \bar{\mathbf{E}}}, \ \bar{\boldsymbol{\alpha}} = \frac{\partial \langle \mathbf{B} \rangle}{\partial \bar{\mathbf{E}}}, \ \bar{\boldsymbol{\mu}} = \frac{\partial \langle \mathbf{B} \rangle}{\partial \bar{\mathbf{H}}}$$

and Dirichlet boundary conditions applied such that:

$$\left[\bar{\mathbf{P}}_m\right]_i = \delta_{im}, \ i, m = (1, .., 12)$$

Computational Approach: The Virtual Element Method[5]

Based on a split of the primary field:

$\boxed{\mathcal{R}_h = \mathcal{R}_\Pi + (\mathcal{R}_h - \mathcal{R}_\Pi)}$ $\mathcal{R}_\Pi$: projected primary fields

At element-level:

$\boxed{\mathcal{R}_\Pi = \sum_{i=1}^{3} \left(\mathbf{N}_\Pi \cdot \mathbf{a}_i^{\mathrm{T}}\right) \mathbf{E}_i}$ with $\mathbf{a}_i$ being the *virtual parameters*

$\mathbf{N}_\Pi = \{1, X, Y, Z\}$, collecting a constant and the node-coordinates

$\Rightarrow$ $\mathbf{a}_i$ are *unknown*, but needed for the global solution

$\boxed{\Rightarrow \text{How to obtain } \mathbf{a}_i?}$

Computational Approach: The Virtual Element Method[5]

Introduction of two constraints to $\mathbf{u}_\Pi$:

1. $\int_{\Omega_e} \nabla \mathcal{R}_\Pi \mathrm{d}V_e \overset{!}{=} \int_{\Omega_e} \nabla \mathcal{R}_h \mathrm{d}V_e$
2. $\frac{1}{n_v} \sum_{k=1}^{n_v} \mathcal{R}_\Pi(\mathbf{X}) \overset{!}{=} \frac{1}{n_v} \sum_{k=1}^{n_v} \mathcal{R}_h(\mathbf{X})$

From that, $\nabla \mathcal{R}_\Pi$ at element-level is obtained by:

$$\nabla \mathbf{u}_\Pi = \frac{1}{\|\Omega_e\|} \sum_{\partial\Omega_e \in \Omega_e} \int_{\partial\Omega_e} \mathbf{u}_h \otimes \mathbf{n} \mathrm{d}A$$
$$\nabla \phi_\Pi = \frac{1}{\|\Omega_e\|} \sum_{\partial\Omega_e \in \Omega_e} \int_{\partial\Omega_e} \phi_h \mathbf{n} \mathrm{d}A$$
$$\nabla \varphi_\Pi = \frac{1}{\|\Omega_e\|} \sum_{\partial\Omega_e \in \Omega_e} \int_{\partial\Omega_e} \varphi_h \mathbf{n} \mathrm{d}A$$

Computational Approach: The Virtual Element Method

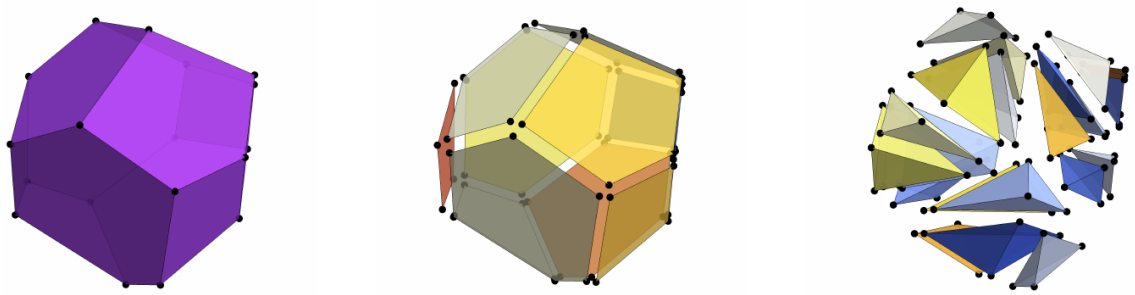

Fig. 4 A virtual element (left), its decomposition into faces (middle) and tetrahedrons (right)

$\Rightarrow$ Split of potential

$$U_{h,e} = \underbrace{W_{c,e}(\nabla \mathcal{R}_\Pi|_e)}_{\textit{consistency}} + \underbrace{\beta\left(W_{c,e}(\nabla \mathcal{R}_h|_e) - W_{c,e}(\nabla \mathcal{R}_\Pi|_e)\right)}_{\textit{stabilization}}$$

Stabilization is computed on triangulated submesh (**Fig. 4**, right)

$\Rightarrow$ Due to linear type of the ansatz: $\langle \cdot \rangle = \int_\Omega (\cdot) \mathrm{d}V = V(\cdot)$

Numerical examples: 3D representative volume element (RVE)

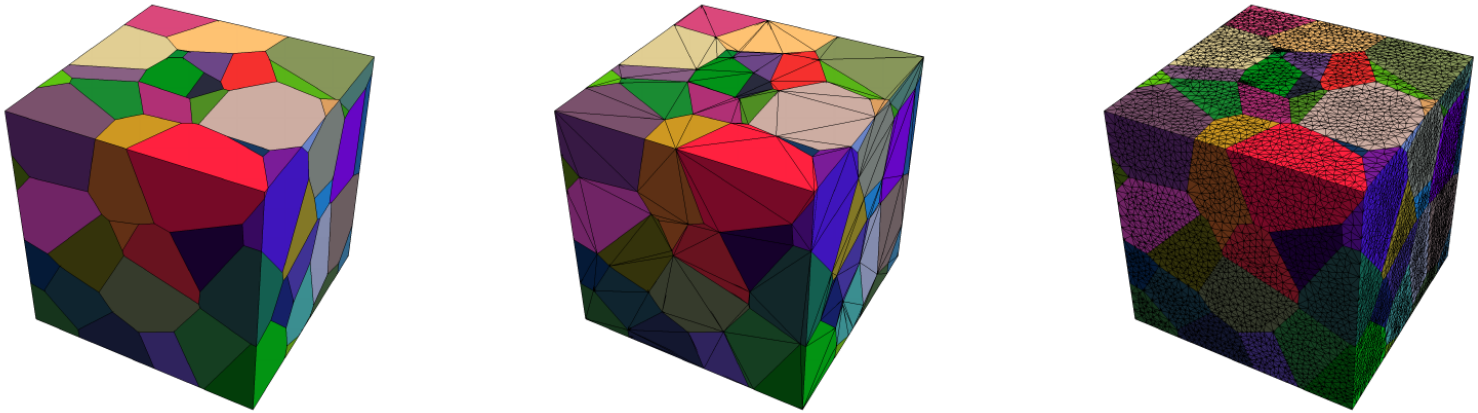

Fig. 5 Artificially generated RVE: VE-Mesh (left), FE-Submesh (middle) and highly refined FE-Mesh (right)

RVE consists of 100 voronoi cells $\Rightarrow$ 100 virtual elements
Submesh has same no. of DOF as VE-Mesh
Highly refined FE-Mesh has $>$ 350k elements (tetrahedral)

Numerical examples: Electro-mechanical coupled problems

$$\bar{\mathbb{G}} = \begin{bmatrix} \bar{\mathbb{C}} & -\bar{\mathbf{e}}^{\mathrm{T}} \\ -\bar{\mathbf{e}} & -\bar{\epsilon} \end{bmatrix}, \left[\bar{\mathbb{G}}\right]_{im} = \left[\mathrm{vec}\{\bar{\boldsymbol{\sigma}}, \bar{\mathbf{D}}\}\right]_{im}, \bar{\boldsymbol{\sigma}} = \langle \boldsymbol{\sigma}|_{\bar{\mathbf{P}}_m} \rangle, \bar{\mathbf{D}} = \langle \mathbf{D}|_{\bar{\mathbf{P}}_m} \rangle$$

with $\bar{\mathbf{P}}_m = \langle \mathbf{P} \rangle$ such that $\left[\bar{\mathbf{P}}_m\right]_i = \delta_{im} \Rightarrow$ 9 independent simulations

Material	MP-ID	Lattice Structure	A^{U}	Point Group
$GaPO_4$	mp-553932	Orthorhombic	1.31	222
$AlPO_4$	mp-4051	Orthorhombic	1.22	222
MoS_2	mp-1434	Trigonal	140.72	$3m$
BN	mp-604884	Hexagonal	244.58	$\bar{6}m2$
$BaNiO_3$	mp-19241	Hexagonal	14.49	$6mm$

Tab. 1 Identification of materials used for studies on electro-mechanical coupled problems

Numerical examples:
Electro-mechanical coupled problems – Computational error

$$\mathcal{E}_C = \left| \frac{\|(\cdot)\|^{\text{Method}}}{\|(\cdot)\|^{\text{fine}}} - 1 \right| 10^2, \text{ with Method: FEM-O1, FEM-O2, VEM-VO}$$

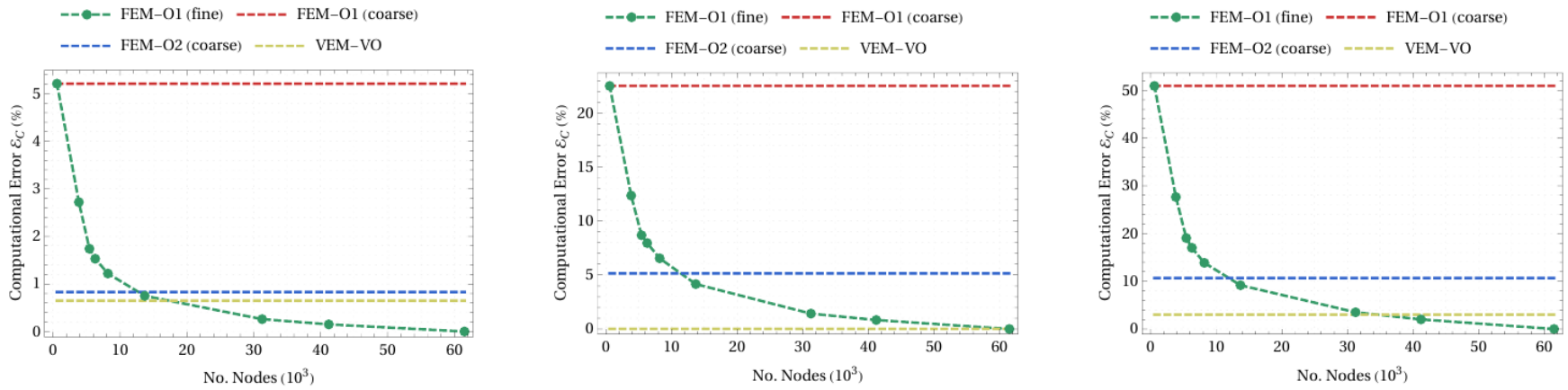

Fig. 6 $\bar{\mathbb{G}}$: quasi-isotropic (left), mildly anisotropic (middle), highly anisotropic (right)

Numerical examples: Macroscopic electro-magneto-mechanical hybrid material

Macroscopic: $\bar{\mathbb{G}} = \begin{bmatrix} \bar{\mathbb{C}} & -\bar{\mathbf{e}}^{\mathrm{T}} & -\bar{\mathbf{q}}^{\mathrm{T}} \\ -\bar{\mathbf{e}} & -\bar{\boldsymbol{\epsilon}} & -\bar{\boldsymbol{\alpha}}^{\mathrm{T}} \\ -\bar{\mathbf{q}} & -\bar{\boldsymbol{\alpha}} & -\bar{\boldsymbol{\mu}} \end{bmatrix}$ $\Rightarrow$ full coupled problem

Microscopic $\mathbb{G} = \begin{bmatrix} \mathbb{C} & -\mathbf{e}^{\mathrm{T}} & -\mathbf{q}^{\mathrm{T}} \\ -\mathbf{e} & -\boldsymbol{\epsilon} & \mathbf{0} \\ -\mathbf{q} & \mathbf{0} & -\boldsymbol{\mu} \end{bmatrix}$ with $\mathbf{e} \neq \mathbf{0}$ or $\mathbf{q} \neq \mathbf{0}$

$\Rightarrow$ No microscopic electro-magnetic coupling for the individual materials

Numerical examples: 3D representative volume element (RVE)

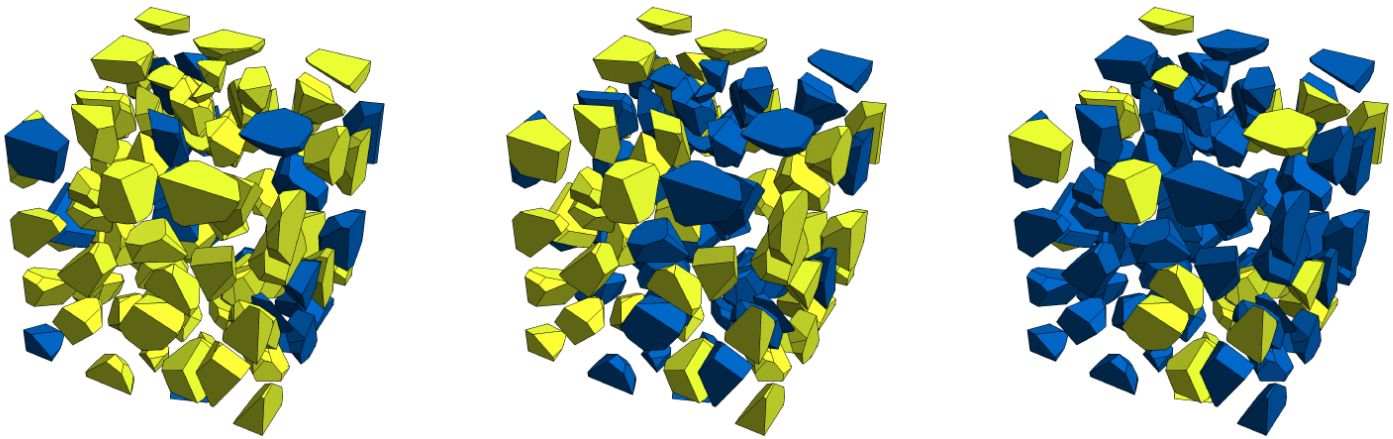

Fig. 7 Artificially generated RVE: Composite microstructure. $BaTiO_3$ (green) and $CoFe_2O_4$ (blue)

Different volume fractions for $CoFe_2O_4$: 0.25, 0.5, 0.75

$\Rightarrow$ macroscopic electro-magnetic coupling $\bar{\boldsymbol{\alpha}} \neq \mathbf{0}$

Maximum magnitude of $\|\bar{\boldsymbol{\alpha}}\|$ is 10^{-3}

Numerical examples: Macroscopic electro-magneto-mechanical hybrid material - parametric study on stabilization influence β

$$\beta_{\text{opt}} := \min_{\beta}\{\mathcal{E}_C\,[\text{VEM} - \text{VO}\,(\mathcal{P}, \beta)]\}$$

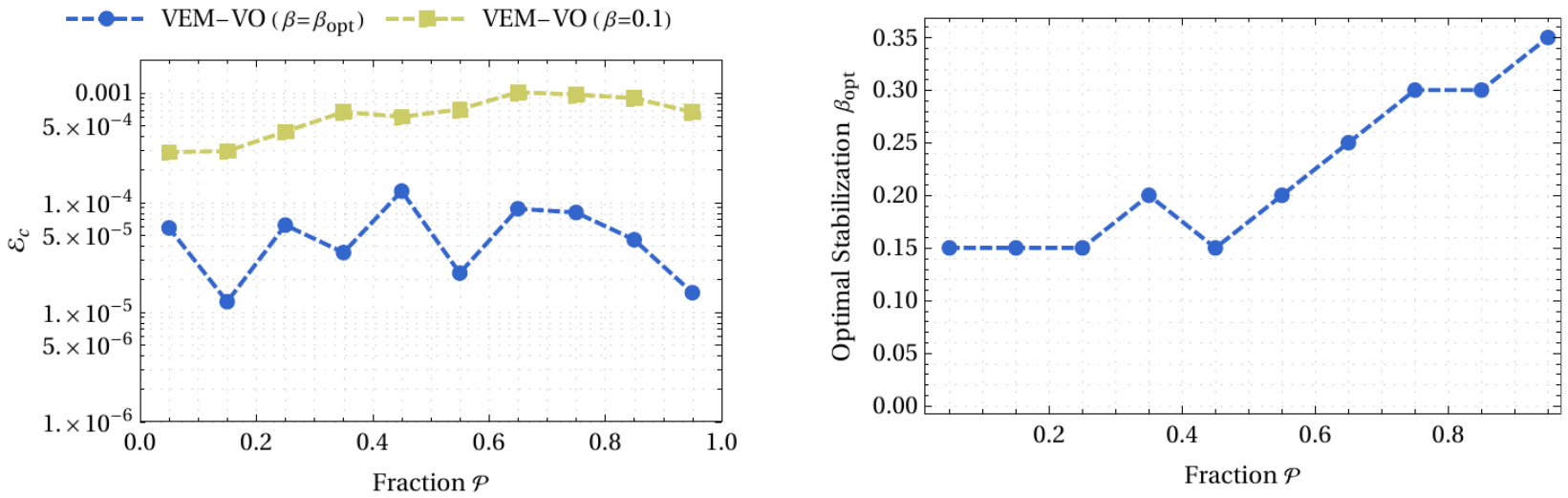

Fig. 8 $\mathcal{E}_C$ versus material fraction $\mathcal{P}$ (left) and β_{opt} versus material fraction $\mathcal{P}$ (right)

Conclusion

→ VE-approaches have the advantage to fit grain-geometries *perfect*
→ VE-approaches outperform linear FE-approaches at same no. of DOF at homogenization procedures for all analysed degrees of elastic anisotropy and all lattice structures (up to a maximum of 12 times less error)
→ VE-approaches show also less error when compared to FE-approaches with quadratic shape functions

⇒ VE-approaches demonstrate high accuracy at small stabilization influences for highly heterogeneous and anisotropic crystalline microstructures

Current Work: Periodic boundary conditions on 3D non-cuboid domains – Periodicity condition[6]

Construction of periodic boundary conditions: $\mathbf{x}^+ - \mathbf{x}^- = \mathbf{F}_M \left(\mathbf{X}^+ - \mathbf{X}^-\right)$
$\rightarrow$ with $\{\mathbf{X}^+, \mathbf{X}^-\} \in \mathbf{B}_c$ (direct constrained nodes on the boundary) leads to $\Delta\mathbf{u}_{bc} = \Delta\mathbf{u}_c$
Where: $\Delta\mathbf{u}_c$ is the difference in displacement of nodes, constrained by $\mathbf{F}_M$, i.e. opposite corner-nodes for a cuboid
Where: $\Delta\mathbf{u}_{bc}$ is the difference in displacement of unconstrained nodes, laying on the boundary of the domain, i.e. nodes on opposite faces for a cuboid
$\rightarrow$ For structured meshes: Node-to-node
$\rightarrow$ For unstructured meshes: Node-to-surface (interpolated displacement on the particular face)
$\Rightarrow$ Drawback for unstructured meshes: additional non-linearity because of the interpolation

Current Work: Periodic boundary conditions on 3D non-cuboid domains – Idea

Consider geometric periodic tesselation as RVE

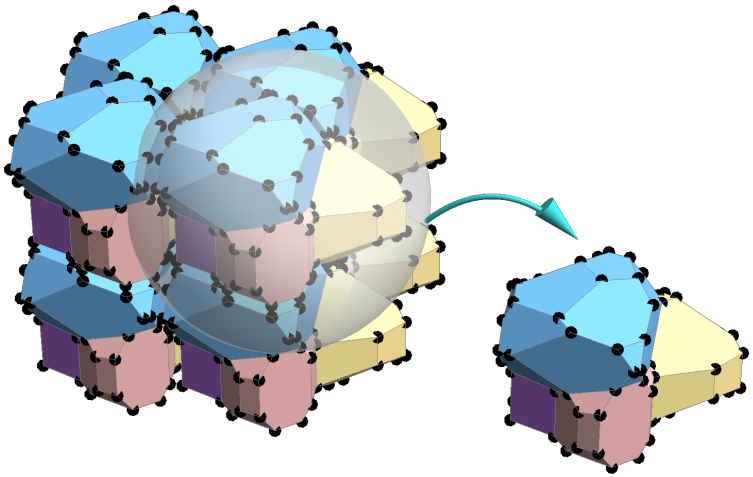

Fig. 9 Stringing together periodic tessellated RVEs and one RVE

If the RVE has geometry that is periodic:

→ Each edge has to have another "pairing edge"

→ Each corner-point has to have matching corner-points

⇒ Node-to-node formulation is possible

Current Work: Periodic boundary conditions on 3D non-cuboid domains – Construction

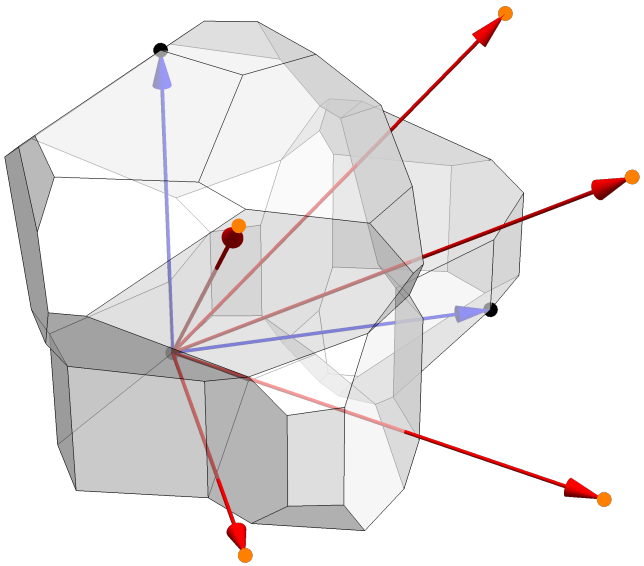

Fig. 10 Physical (black) and artificial (orange) corner-nodes of the RVE

Find physical "corner"-nodes:

→ Add "artificial corner"-nodes

→ Constrain by $\mathbf{F}_M$

→ Constrain remaining boundary nodes s.t. $\Delta\mathbf{u}_{bc} = \Delta\mathbf{u}_c$

Current Work: Periodic boundary conditions on 3D non-cuboid domains – How to evaluate?

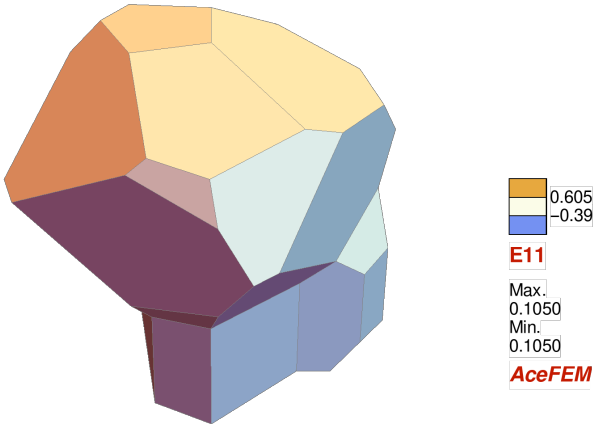

Fig. 11 Green-Lagrange Strain ($\mathbf{E}_{11}$ component) of the RVE

Evaluate Hill's condition:

- → Isotropic material (geometric non-linear)
- → $\langle \mathbf{F}_m \rangle = \mathbf{F}_M$
- → $\mathbf{P}_m = \text{const.}$
- → applied $\mathbf{F}_M = \mathbf{1} + 0.1\mathbf{e}_1 \otimes \mathbf{E}_1$

References

[1] Herbst, S., Maier, H.J.; Nürnberger, F.: Strategies for the Heat Treatment of Steel-Aluminium Hybrid Components. *HTM Journal of Heat Treatment and Materials*, 73(5), 2018.

[2] Böhm, C., Hudobivnik, B., Marino, M., Wriggers, P.: Electro-magneto-mechanically response of polycrystalline materials: Computational Homogenization via the Virtual Element Method. *Computer Methods in applied Mechanics and Engineering* 380, 113775, 2021.

[3] Schröder, J., Labusch, M., Keip, M.-A.: "Algorithmic two-scale transition for magneto-electro-mechanically coupled problems: FE2-scheme: Localization and homogenization." *Computer Methods in applied Mechanics and Engineering* 302, 253-280, 2016.

[4] Korelc, J., Wriggers, P.: Automation of Finite Element Methods. *Springer International Publishing, Switzerland*, 2016.

[5] Beirão da Veiga, L., et al.: "The hitchhiker's guide to the virtual element method." *Mathematical models and methods in applied sciences* 24(8), 1541-1573, 2014.

[6] Šolinc, U., Korelc, J.: "A simple way to improved formulation of FE^2 analysis." *Computational mechanics* 56(5), 905-915, 2015.

Acknowledgement

CB and PW acknowledge the financial support to this work by the German Research Foundation (DFG, Deutsche Forschungsgemeinschaft) with the collaborative research centre 1153 (SFB 1153) "Process chain for the production of hybrid high-performance components through tailored forming" with the subproject C04 "Modelling and Simulation of the Joining Zone", project number 252662854. MM acknowledges the Italian Ministry of Education, University and Research (MIUR) for funding in the framework of the Rita Levi Montalcini Program (Programma per Giovani ricercatori anno 2017 Rita Levi Montalcini). BH and PW gratefully acknowledge financial support to this work by the German Research Foundation (DFG) with the cluster of excellence PhoenixD (EXC 2122).

SFB 1153

Programma Rita Levi Montalcini

Leibniz Universität Hannover

PhoenixD
Photonics · Optics · Engineering
Innovation Across Disciplines